Bharat Laxmi[1], *Khem Chand*[1*], *Pankaj Thakur*[2**]

INFLUENCE OF MAGNETIC FIELD AND HEAT SOURCE ON ROTATING HYBRID NANOFLUID FLOW OVER A STRETCHING/SHRINKING PERMEABLE SHEET

UTICAJ MAGNETNOG POLJA I IZVORA TOPLOTE NA ROTIRAJUĆI PROTOK HIBRIDNOG NANOFLUIDA PREKO ISTEGNUTE/SKUPLJENE PROPUSNE TRAKE

Originalni naučni rad / Original scientific paper
Rad primljen / Paper received: 24.04.2025
https://doi.org/10.69644/ivk-2026-01-0149

Adresa autora / Author's address:
[1)] Department of Mathematics & Statistics, Himachal Pradesh University, Summer Hill, Shimla-171005, India
K. Chand https://orcid.org/0000-0002-6360-7729 ,
[*]email: khemthakur99@gmail.com
[2)] Department of Mathematics, ICFAI University Baddi, Solan, Himachal Pradesh, India
P. Thakur https://orcid.org/0000-0001-8119-2697 ,
[**]email: pankajthakur15@yahoo.co.in

Keywords
- rotating flow
- hybrid nanofluid
- stretching/shrinking sheet
- viscous dissipation
- heat source

Ključne reči
- rotirajući protok
- hibridni nanofluid
- istegnuta/skupljena traka
- viskozna disipacija
- izvor toplote

Abstract

In this paper we examine the heat transfer characteristics of three-dimensional rotating flow of convective hybrid nanofluid flow over a stretching/shrinking permeable sheet in the presence of a magnetic field and heat source effects. Hybrid nanofluids exhibit promising characteristics for various applications, particularly in enhancing heat transfer rates. The hybrid nanofluid used in the paper is alumina (Al_2O_3) and copper (Cu) with water (H_2O) serving as the base fluid. The governing nonlinear partial differential equations are transformed into linear ordinary differential equations using similarity transformations and are numerically solved using the bvp4c function in MATLAB® software. The influence of various governing parameters on the velocities and temperature profiles is represented through graphs. The parameters include magnetic field, Darcy permeability, Eckert number, suction effects, Biot number, rotating parameter, and heat source parameter. Further, the impact of suction parameter on the skin friction and reduced heat transfer is also examined.

Izvod

U ovom radu istražujemo karakteristike trodimenzionalnog rotirajućeg protoka konvekcionog protoka hibridnog nanofluida preko istegnute/skupljene propusne trake, u prisustvu magnetnog polja i izvora toplote. Hibridni nanofluidi pokazuju obećavajuće karakteristike kod raznih primena, posebno za poboljšanje brzina prenosa toplote. Hibridni nanofluid u radu je oksid aluminijuma (Al_2O_3) i bakar (Cu) sa vodom (H_2O), koja je zapravo bazni fluid. Osnovne nelinearne parcijalne diferencijalne jednačine se transformišu u obične linearne diferencijalne jednačine transformacijama sličnosti i rešavaju se numerički funkcijom bvp4c softvera MATLAB®. U radu su grafički predstavljeni uticaji raznih osnovnih parametara na brzine i profile temperature. Među obrađenim parametrima su magnetno polje, Darsi permeabilnost, Ekertov broj, uticaji usisavanja, Biot-ov broj, parametar rotacije, i parametar izvora toplote. Takođe se proučava uticaj parametra usisavanja na površinsko trenje i smanjenje prenosa toplote.

INTRODUCTION

Traditional research on nanofluids defines them as fluids containing dispersed nanometre-sized solid particles, rods, or tubes in conventional heat transfer fluids like water, engine oil, ethylene glycol, or kerosene. Numerous studies have explored how particle size, shape, concentration, and thermophysical properties affect the heat transfer rate of nanofluids. This area of research has garnered significant interest due to the exciting thermal properties and potential applications of nanofluids. Recently, experimental studies have focused on hybrid nanofluids, which involve two types of nanoparticles dispersed in a base fluid. These hybrid nanofluids offer advantages by combining each particle type's positive features and mitigating their drawbacks through synergistic effects. This emerging class of nanofluids has vast potential applications across various heat transfer fields, including microelectronics, microfluidics, transportation, manufacturing, medical, defence, acoustics, naval structures, and propulsion. When properly dispersed, hybrid nanofluids can provide significant benefits beyond their exceptionally high effective thermal conductivity. They are known for their superior heat transfer rates compared to traditional fluids, and introducing hybrid nanofluids aims to enhance these properties further. This study focuses on analysing the heat transfer characteristics of hybrid nanofluids over a stretching sheet.

Over the past few years, research into a novel approach to addressing boundary layer flow problems has focused on enhancing heat transfer in hybrid nanofluids. In response to the growing demand for increased heat transfer rates across various industries, scientists have experimented with incorporating numerous solid nanoparticles into different base fluids. Initiating study on three-dimensional rotating viscous flow induced by a stretching surface is presented by Wang /1/. His problem is governed by an interesting parameter λ that signifies the ratio of rotation to the stretching rate. Devi

and Devi /2/ numerically investigate the hydromagnetic hybrid Cu-Al_2O_3/water nanofluid flow over a permeable stretching sheet with suction. Ramzan et al. /3/ have studied three-dimensional second-grade nanofluid flow with effects of thermal radiation and mixed convection over an exponentially stretching surface in the presence of convective boundary conditions. Mustafa et al. /4/ have studied rotating flow of a magnetite-water nanofluid over a stretching surface in the presence of nonlinear thermal radiation. Hayat and Nadeem /5/ studied the enhancement of heat transfer with Ag-CuO/water hybrid nanofluid. Waini et al. /6/ studied the radiation impacts on a hybrid nanofluid with a nonlinear stretched/shrunk layer. Wang et al. /7/ investigated the three-dimensional nanofluid motion with convective boundary condition in the presence of nonlinear thermal radiation over a stretching sheet.

It is crucial to acknowledge the significant impact of thermal radiation on exceptionally high-temperature applications. In many industrial operations, temperatures can reach very high levels, making sensitivity to thermal radiation an absolute necessity for developing appropriate machinery. Thermal radiation also has abundant real-world applications in the trade sector, such as in the production of glass and the design of furnaces. Additionally, it plays a crucial role in the aerospace industry, where it is utilised in the generation of solar radiation, spacecraft, launch systems, combustion engines, and boat steam turbines. Hayat et al. /8/ have numerically studied the rotating flow of Ag-CuO/water hybrid nanofluid with radiation and partial slip boundary effects. Aly and Pop /9/ studied the two-dimensional steady flow over a permeable stretching/shrinking sheet of a hybrid nanofluid in the presence of suction. Later, Anuar et al. /10/ studied the hybrid nanofluid steady rotating flow over a stretched/shrunk surface in the presence of radiation. Moreover, Khashi et al. /11/ investigated steady hybrid nanofluid flow on a rotating stretching/shrinking surface in the presence of convective boundary and velocity slip conditions. Teh and Asghar /12/ studied the three-dimensional rotating MHD hybrid nanofluid flow over a stretching/shrinking surface in the presence of Joule heating. Joule heating is a process in which heat is created by passing current through a conductor.

Viscous dissipation is the process by which work done by viscous forces converts the kinetic energy of a fluid into thermal energy. In the context of energy dissipation due to viscous heating, the large velocity gradients within the boundary layer play a significant role. In the subsequent year, Hafidzuddin and Alias /13/ investigate the Navier slip flow phenomenon induced by magnetohydrodynamics (MHD) on a nonlinearly stretching and shrinking sheet in the presence of suction. Their findings reveal that suction amplifies skin friction, while the slip parameter reduces shear wall stress. Furthermore, they observe that the stretching sheet exhibits a narrower range of dual solutions compared to the shrinking case. Further, Asghar et al. /14/ have studied three-dimensional magnetised rotating flow of hybrid nanofluid under the effect of thermal radiation. Similarly, Wahid et al. /15/ conducted a numerical study on the influence of convective boundary conditions and heat radiation on the flow of magnetic nanofluids (MNFs) through a permeable moving plate. They analysed elevated levels of thermal radiation and Biot number to assess the heat transfer performance of MNFs, concluding that higher values of these parameters effectively augment the heat transfer rate. Recently, Raju et al. /16/ examined unsteady and incompressible magnetohydrodynamic rotating free convection flow of viscoelastic fluid with simultaneous heat and mass transfer near an infinite vertical oscillating porous plate under the influence of a uniform transverse magnetic field, including Hall current effects. They determined that as the radiation parameters increase, the resulting velocity strengthens and experiences deceleration within the flow field. Conversely, they noted that the secondary velocity component increases with higher rotation parameters. Asghar et al. /17/ investigates the dual solutions of convective rotating flow of hybrid nanofluid over a stretching/shrinking sheet.

Building on previous research, this study theoretically analyses the heat transfer characteristics of three-dimensional convective rotating flow of hybrid nanofluid under the influence of viscous dissipation and heat source effects over a stretching/shrinking permeable sheet in the presence of a magnetic field and heat source. The hybrid nanofluid consists of alumina (Al_2O_3) and copper (Cu) nanoparticles dispersed in a water-based fluid. The aim of taking these two nanoparticles is that both have a good capacity of taking high thermal conductivity, which means they transfer heat effectively. The governing partial differential equations (PDEs) describing the system are transformed into a set of nonlinear coupled ordinary differential equations (ODEs) using a suitable similarity transformation technique. These transformed ODEs are numerically solved using MATLAB's bvp4c function, a boundary value problem solver. The solutions for both velocity and temperature fields are numerically evaluated through MATLAB. The study examines the impact of various parameters in the governing equations, including magnetic field strength, viscous dissipation, heat source intensity, and suction/injection rates, on the velocity and temperature profiles of the flow. These effects are graphically illustrated to provide a comprehensive discussion of the flow characteristics and thermal behaviour under different conditions. The results for skin friction and Nusselt number are also illustrated graphically.

MATHEMATICAL FRAMEWORK

A steady incompressible 3-D hybrid nanofluid flow over a stretching/shrinking sheet is considered. The Cartesian coordinates for the sheets are taken as x-axis and y-axis in the $z = 0$ plane. Let (u, v, w) be the velocity elements in the (x, y, z) directions, respectively, as shown in Fig. 1. A uniform magnetic field B_0 is applied perpendicular to the sheet. The sheet is stretched through the x-coordinate system, and at $z \geq 0$, half of the region is taken up by the fluid. The surface velocity $U_w(x) = ax$ is taken for stretching/shrinking sheet in the x-direction, where $a > 0$ is the stretching rate parameter. Here, $\lambda > 0$ is taken as the stretching constant, whereas $\lambda < 0$ is the shrinking constant, $\lambda = 0$ refers to a motionless sheet. The temperature of the fluid $T_w(x) = T_\infty + T_0x^2$, where T_0 is a positive constant temperature of the fluid at the origin and

T_∞ is the free stream temperature of the fluid. The entire system rotates at constant angular velocity Ω along a perpendicular direction to the surface z-axis.

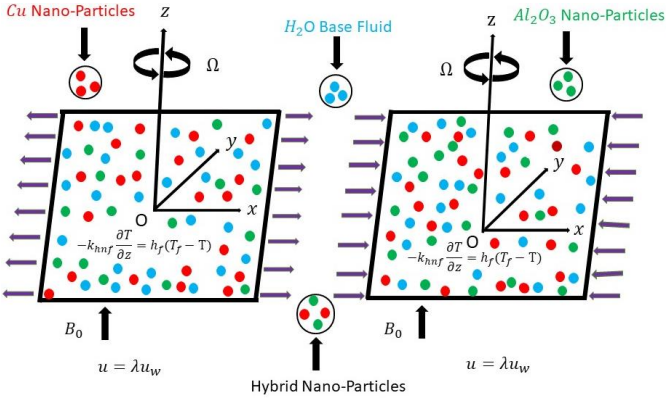

Figure 1. Physical model for stretching/shrinking sheet.

Under boundary layer approximation and constant fluid property assumption, the continuity, momentum, and energy equations for the flow by following /10-11/, are as follows:

$$\frac{\partial u}{\partial x}+\frac{\partial v}{\partial y}+\frac{\partial w}{\partial z}=0\,, \tag{1}$$

$$u\frac{\partial u}{\partial x}+v\frac{\partial u}{\partial y}+w\frac{\partial u}{\partial z}-2\Omega v=\frac{\mu_{hnf}}{\rho_{hnf}}\frac{\partial^2 u}{\partial z^2}-\frac{\sigma_{hnf}}{\rho_{hnf}}B_0^2u-\frac{\mu_{hnf}}{\rho_{hnf}k'}u, \tag{2}$$

$$u\frac{\partial u}{\partial x}+v\frac{\partial u}{\partial y}+w\frac{\partial u}{\partial z}-2\Omega u=\frac{\mu_{hnf}}{\rho_{hnf}}\frac{\partial^2 v}{\partial z^2}-\frac{\sigma_{hnf}}{\rho_{hnf}}B_0^2v-\frac{\mu_{hnf}}{\rho_{hnf}k'}v, \tag{3}$$

$$u\frac{\partial T}{\partial x}+v\frac{\partial T}{\partial y}+w\frac{\partial T}{\partial z}=\frac{k_{hnf}}{(\rho c)_{hnf}}\frac{\partial^2 T}{\partial z^2}+\frac{\mu_{hnf}}{(\rho C_p)_{hnf}}\left(\frac{\partial u}{\partial z}\right)^2+$$
$$+\frac{Q_0}{(\rho C_p)_{hnf}}(T-T_\infty)+\frac{\sigma_{hnf}}{\rho_{hnf}}B_0^2u^2\,. \tag{4}$$

Associated boundary conditions by following /2, 9/ are as follows:

$$u=\lambda u_w(x),\quad v=0,\quad w=w_w,$$
$$-k_{hnf}\frac{\partial T}{\partial z}=h_f(T_f-T)\quad\text{at}\quad z=0,$$
$$u=0,\quad v=0,\quad T\to T_\infty,\quad\text{as}\quad r\to\infty\,. \tag{5}$$

In the above-mentioned expressions, λ denotes stretching ($\lambda>0$) or shrinking ($\lambda<0$) parameter, $w_w=-\sqrt{(av_f}S)$ is the constant mass velocity, where S is suction/injection parameter, such that $S>0$ for suction, and $S<0$ for injection, and h_f is a heat transfer coefficient. To nondimensionalise the governing equations, we introduce the following similarity variables: η, dimensionless velocity variable f, and temperature variable θ as:

$$u=axf'(\eta),\quad v=axg(\eta),\quad w=-\sqrt{av_f}\,f(\eta),$$
$$\theta(\eta)=\frac{T-T_\infty}{Tf-T_\infty},\quad \eta=z\sqrt{\frac{a}{v_f}}. \tag{6}$$

By substituting Eq.(6) into Eq.(1), the continuity equation is satisfied, and the remaining equations are transformed into ODEs as shown below,

$$\left(\frac{\mu_{hnf}/\mu_f}{\rho_{hnf}/\rho_f}\right)f'''+ff''-f'^2+2\omega g-(M+K)f'=0\,, \tag{7}$$

$$\left(\frac{\mu_{hnf}/\mu_f}{\rho_{hnf}/\rho_f}\right)g'''+fg'-f'g-2\omega f'-(M+K)g=0\,, \tag{8}$$

$$\frac{1}{Pr}\frac{(\rho C_p)_f}{(\rho C_p)_{hnf}}\frac{k_{hnf}}{k_f}\theta''+f\theta'+\frac{\mu_{hnf}(\rho C_p)_f}{\mu_f(\rho C_p)_{hnf}}Ecf''^2+$$
$$+Q\theta-\frac{\sigma_{hnf}(\rho C_p)_f}{(\rho C_p)_{hnf}}MEcf'^2=0\,, \tag{9}$$

and the boundary conditions transform to

$$f(0)=S,\ g(0)=0,\ f'(0)=\lambda,\ -Kh\theta'(0)=B[1-\theta(0)],$$
$$f'(\eta)\to0,\ g(\eta)\to0,\ \theta\to0\ \text{ as }\ \eta\to\infty\,, \tag{10}$$

where: $\omega=\Omega/a$ is rotation parameter; $M=\sigma_{hnf}B_0^2/\rho_{hnf}a$ is magnetic field parameter; $K=\mu_{hnf}/\rho_{hnf}k^*a$ is Darcy permeability; $Pr=(\mu C_p)_f/k_f$ is Prandtl number; $B=h_f/k_f\sqrt{(v_f/a)}$ is Biot number parameter; $Ec=U_w^2/(T_f-T_\infty)(C_p)_f$ is the Eckert number (viscous dissipation); and $Q=Q_0/(\rho C_p)_{hnf}a$ is heat source parameter.

SOME IMPORTANT CHARACTERISTICS OF THE FLOW FIELD

Local skin friction coefficient

The local skin friction coefficients C_{fx} and C_{fy} along x and y-axis, respectively, are defined as

$$C_{fx}=\frac{\mu_{hnf}}{\mu_fU_w^2}\left(\frac{\partial u}{\partial z}\right)_{z=0},\quad\text{and}\quad C_{fy}=\frac{\mu_{hnf}}{\mu_fU_w^2}\left(\frac{\partial v}{\partial z}\right)_{z=0}. \tag{11}$$

The skin friction coefficient in terms of transformed variables, Eqs.(6) and (11), can be obtained as

$$(Re_x)^{1/2}C_{fx}=\frac{\mu_{hnf}}{\mu_f}f''(0)\,,$$

and

$$(Re_x)^{1/2}C_{fy}=\frac{\mu_{hnf}}{\mu_f}g'(0)\,, \tag{12}$$

where: $f''(0)$ and $g'(0)$ are obtained using Eqs.(7) and (8).

Dimensionless coefficient of heat transfer (Nusselt number)

The local Nusselt number Nu_x is defined as

$$Nu_x=\frac{xk_{hnf}}{k_f(T_f-T_\infty)}\left(-\frac{\partial T}{\partial z}\right)_{z=0}. \tag{13}$$

The dimensionless expression for the Nusselt number in terms of transformation variables, Eq.(6), and using Eq.(13) turns out to be

$$(Re_x)^{-1/2}Nu_x=\frac{-k_{hnf}}{k_f}\theta'(0)\,, \tag{14}$$

where: $\theta'(0)$ is obtained from Eq.(9); however, $Re_x=U_w(x)x/v_f$ is the local Reynolds number; $f''(0)$ and $-\theta'(0)$ are velocity and temperature gradients, respectively.

RESULTS AND DISCUSSION

To gain a clear understanding of the physical problem, we numerically examine the flow characteristics in the x- and y-directions, along with the heat transfer properties, using both hybrid nanofluid (Cu-Al_2O_3/water) and nanofluid (Cu/water) over a three-dimensional stretching ($\lambda>0$) and shrinking ($\lambda<0$) sheet. The numerical calculations for the velocity profiles $f'(\eta)$, $g(\eta)$, and temperature profile $\theta(\eta)$ are performed for various values of governing parameters. These

parameters include the magnetic field parameter M, porosity parameter K, Prandtl number Pr, heat source parameter Q, solid volume fractions of Cu (ϕ_{s2}), Eckert number Ec, suction parameter S, stretching/shrinking parameter λ, rotation parameter ω, Biot number B. Additionally, the results for physical quantities such as local skin friction coefficients C_{fx} and C_{fy}, and Nusselt number Nu_x are calculated and presented through graphs.

Impact on velocity profile $f'(\eta)$

In this subsection, the impacts of various governing parameters on velocity profiles $f'(\eta)$ and $g(\eta)$ are analysed graphically. Figure 2 illustrates the influence of the magnetic field parameter M on dimensionless velocity $f'(\eta)$ over a stretching/shrinking sheet. It is observed that increasing the magnetic field parameter reduces the velocity at all points in the flow field over the stretching sheet, whereas it increases the velocity over the shrinking sheet. This occurs because the application of a transverse magnetic field creates a resistive force (Lorentz force), similar to a drag force, that opposes the fluid flow and reduces its velocity. A similar effect is seen in Fig. 3, where velocity $g(\eta)$ decreases with increasing magnetic field parameter M. Figures 4 and 5 demonstrate that an increase in rotation parameter ω directly affects both velocity profiles $f'(\eta)$ and $g(\eta)$. This is due to the increase in angular thickness of the momentum boundary layer with higher rotational parameter values, indicating a consistent approach in the fluid problem with hybrid nanofluids. Physically, the rapid movement of nanoparticles contributes to the enhanced velocity of hybrid nanofluid flow. Figure 6 shows the effect of permeability parameter K on the velocity profile. The figure indicates that the velocity in

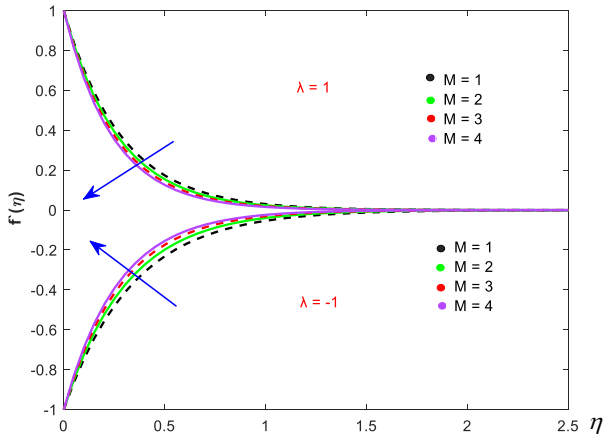

Figure 2. Velocity profiles $f'(\eta)$ for various magnetic field parameter M when: $K = 0.5$; $Ec = 0.1$; $Q = 0.1$; $S = 2.2$; $Pr = 6.2$; $B = 0.1$; $\omega = 0.5$; $\lambda = 1, -1$; $\phi_{s1} = 0.01$; $\phi_{s2} = 0.01$.

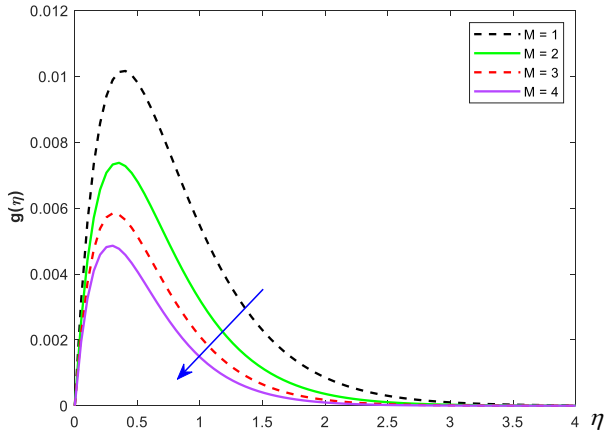

Figure 3. Velocity profiles $g(\eta)$ for various magnetic field parameter M when: $K = 0.5$; $Ec = 0.1$; $Q = 0.1$; $S = 2.2$; $Pr = 6.2$; $B = 0.1$; $\omega = 0.5$; $\lambda = -1$; $\phi_{s1} = 0.01$; $\phi_{s2} = 0.01$.

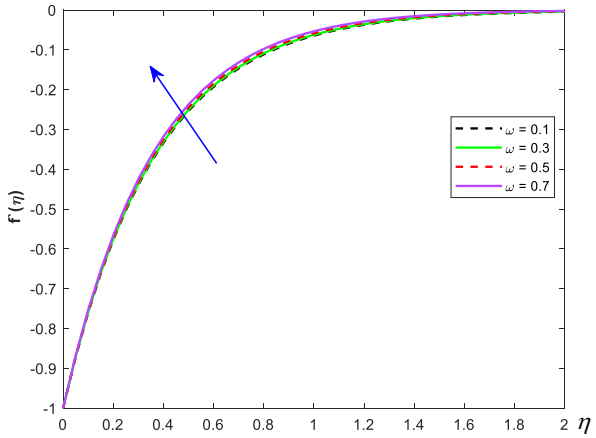

Figure 4. Velocity profiles $f'(\eta)$ for various rotation parameter ω when: $K = 0.5$; $Ec = 0.1$; $Q = 0.1$; $S = 2.2$; $Pr = 6.2$; $B = 0.1$; $M = 0.5$; $\lambda = -1$; $\phi_{s1} = 0.01$; $\phi_{s2} = 0.01$.

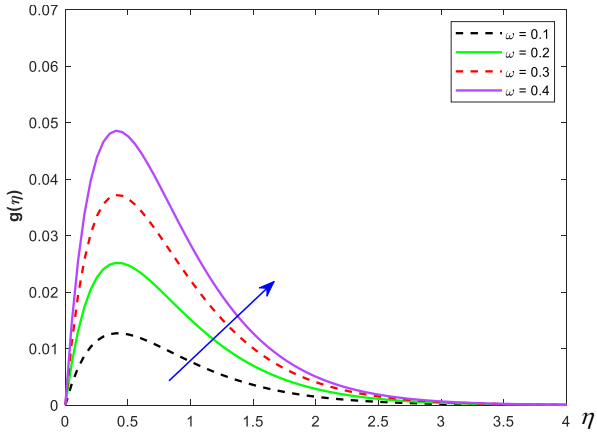

Figure 5. Velocity profiles $g(\eta)$ for various rotation parameter ω when: $K = 0.5$; $Ec = 0.1$; $Q = 0.1$; $S = 2.2$; $Pr = 6.2$; $B = 0.1$; $M = 0.5$; $\lambda = -1$; $\phi_{s1} = 0.01$; $\phi_{s2} = 0.01$.

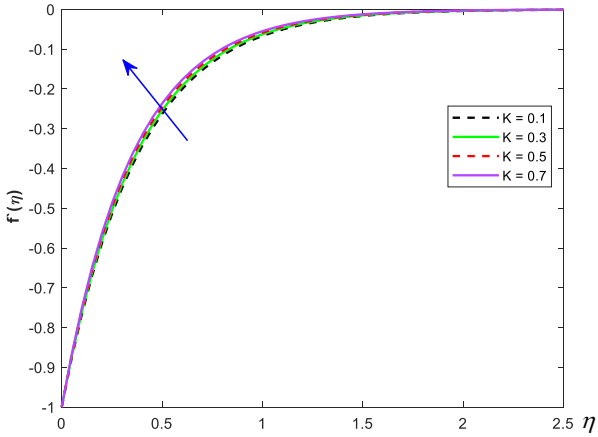

Figure 6. Velocity profiles $f'(\eta)$ for various permeability parameter K when: $\omega = 0.5$; $Ec = 0.1$; $Q = 0.1$; $S = 2.2$; $Pr = 6.2$; $B = 0.1$; $M = 0.5$; $\lambda = -1$; $\phi_{s1} = 0.01$; $\phi_{s2} = 0.01$.

the x-direction increases with higher permeability parameter values. Increased permeability reduces the drag force on the fluid, allowing it to move more freely and resulting in higher velocities. Conversely, Fig. 7 shows that the velocity in the y-direction decreases with increasing permeability parameter values. Figure 8 illustrates that the velocity profile in the x-direction increases with higher values of suction parameter

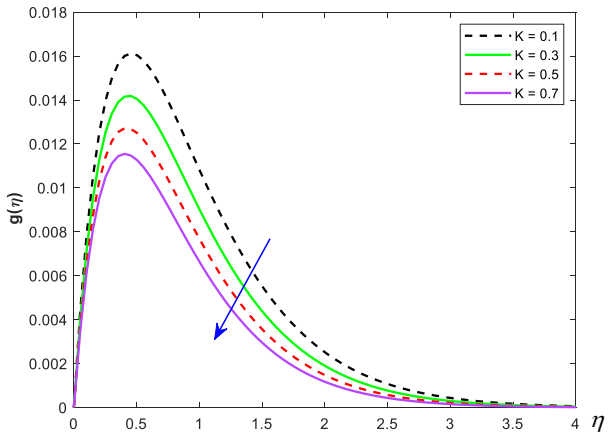

Figure 7. Velocity profiles $g(\eta)$ for various permeability parameter K when: $\omega = 0.5$; $Ec = 0.1$; $Q = 0.1$; $S = 2.2$; $Pr = 6.2$; $B = 0.1$; $M = 0.5$; $\lambda = -1$; $\phi_{s1} = 0.01$; $\phi_{s2} = 0.01$.

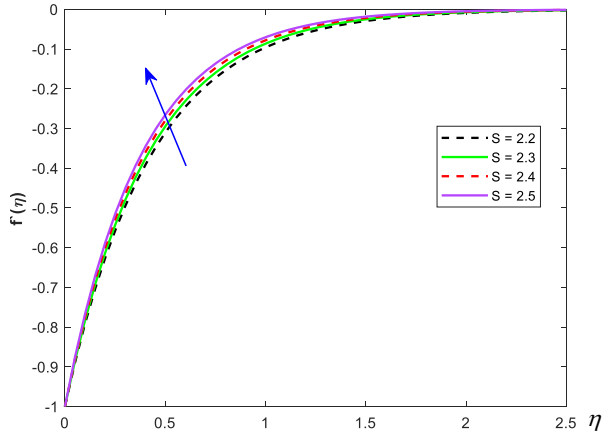

Figure 8. Velocity profiles $f'(\eta)$ for various suction parameter S when: $\omega = 0.5$; $Ec = 0.1$; $Q = 0.1$; $K = 0.5$; $Pr = 6.2$; $B = 0.1$; $M = 0.5$; $\lambda = -1$; $\phi_{s1} = 0.01$; $\phi_{s2} = 0.01$.

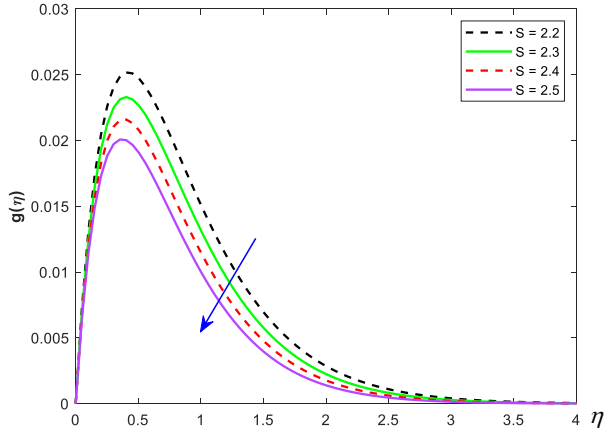

Figure 9. Velocity profiles $g(\eta)$ for various suction parameter S when: $\omega = 0.5$; $Ec = 0.1$; $Q = 0.1$; $K = 0.5$; $Pr = 6.2$; $B = 0.1$; $M = 0.5$; $\lambda = -1$; $\phi_{s1} = 0.01$; $\phi_{s2} = 0.01$.

S, which makes the momentum boundary layer thinner. In contrast, Fig. 9 shows that the velocity profile in the y-direction decreases as suction parameter S increases. Figure 10 demonstrates that an increase in copper volume fraction parameter ϕ_{s2} leads to an enhancement in the velocity profile $f'(\eta)$ in x-direction. This can be attributed to the fact that the addition of copper to a base fluid such as water enhances its thermophysical properties, including thermal diffusivity, thermal conductivity, and heat transfer coefficient. These improvements in the base fluid's properties result in an increased velocity profile in the x-direction. Conversely, Fig. 11 indicates that the velocity profile $g(\eta)$ in the y-direction decreases with increasing value of copper volume fraction parameter ϕ_{s2}.

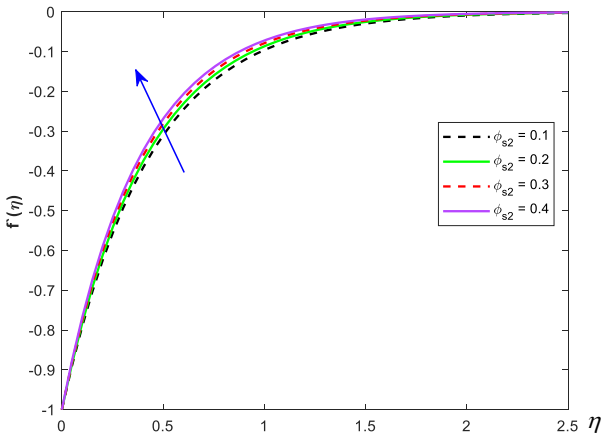

Figure 10. Velocity profiles $f'(\eta)$ for various volume fraction parameter ϕ_{s2} when: $\omega = 0.5$; $Ec = 0.1$; $Q = 0.1$; $K = 0.5$; $Pr = 6.2$; $B = 0.1$; $M = 0.5$; $\lambda = -1$; $S = 2.2$; $\phi_{s1} = 0.01$.

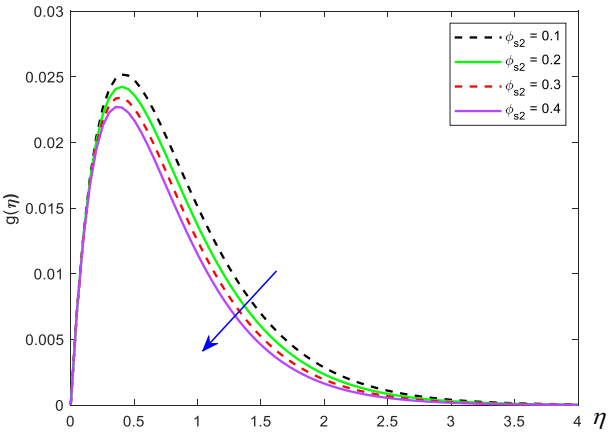

Figure 11. Velocity profiles $g(\eta)$ for various volume fraction parameter ϕ_{s2} when: $\omega = 0.5$; $Ec = 0.1$; $Q = 0.1$; $K = 0.5$; $Pr = 6.2$; $B = 0.1$; $M = 0.5$; $\lambda = -1$; $S = 2.2$; $\phi_{s1} = 0.01$.

Impact on temperature profile $\theta(\eta)$

In this subsection, the impacts of various governing parameters on the temperature profile $\theta(\eta)$ are studied graphically. The influence of the magnetic field parameter M on the temperature profile is shown in Fig. 12. It is found that the temperature decreases with an increasing value of the magnetic field parameter. This indicates that a stronger magnetic field tends to reduce the temperature in the boundary layer. Figure 13 analyses the effect of the suction parameter on the temperature profile. It is clear from the figure that an

increase in the suction parameter leads to a reduction in the temperature profiles. Consequently, the thermal boundary layer thickness diminishes with higher suction rates. The enhancement of the heat source parameter results in an expansion of the temperature profile $\theta(\eta)$, as shown in Fig. 14. This implies that the presence of a heat source increases the temperature within the boundary layer. Figure 15 demonstrates that with an increase in the Prandtl number Pr the temperature profile decreases. An increase in the Prandtl number reduces the thermal boundary layer thickness. When the Prandtl number is small, heat diffuses quickly compared to the velocity. In the presence of viscous dissipation, the effect of the Eckert number Ec on the temperature profile of the hybrid nanofluid is shown in Fig. 16. It is observed that with an increase in Eckert number, the temperature profile expands along the stretching/shrinking sheet. This is due to the viscous dissipation effects, which cause thermal reversal in the boundary layer near the surface of the stretching/shrinking wedge. The Biot number is a dimensionless quantity that compares the relative importance of internal to external thermal resistances. As the Biot number increases, hot fluids heat the lower surface of a stretching sheet, enhancing convective heat transfer and consequently raising the temperature. This phenomenon is illustrated in Fig. 17, which demonstrates that the enhancement of the Biot number B enhances the thermal boundary layer, leading to an enhancement of the temperature profile. Moreover, since the Biot number is directly proportional to the heat transfer coefficient, an increase in the Biot number results in a significant increase in the non-dimensional rate of heat transfer for both types of nanofluids. Figure 18 demonstrates that an increase in the copper volume fraction parameter ϕ_{s2} leads to an enhancement in the temperature profile $\theta(\eta)$.

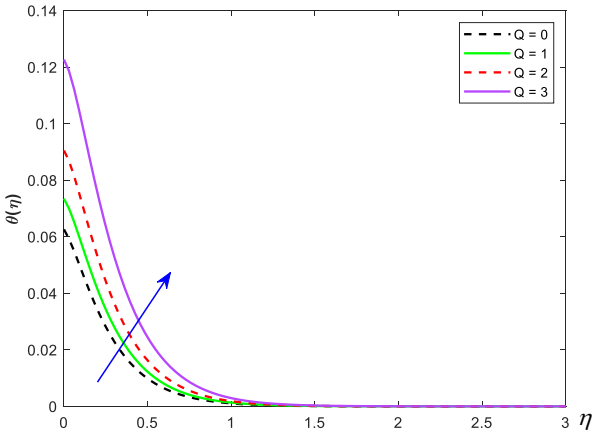

Figure 14. Temperature profiles $\theta(\eta)$ for various heat source parameter Q when: $\omega = 0.5$; $Ec = 0.1$; $M = 0.5$; $K = 0.5$; $S = 2.2$; $Pr = 6.2$; $B = 0.1$; $\lambda = -1$; $\phi_{s1} = 0.01$; $\phi_{s2} = 0.01$.

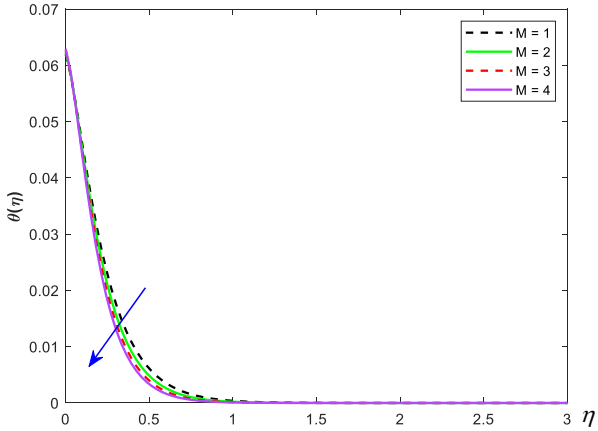

Figure 12. Temperature profiles $\theta(\eta)$ for various magnetic field parameter M when: $\omega = 0.5$; $Ec = 0.1$; $Q = 0.1$; $K = 0.5$; $Pr = 6.2$; $B = 0.1$; $\lambda = -1$; $S = 2.2$; $\phi_{s1} = 0.01$; $\phi_{s2} = 0.01$.

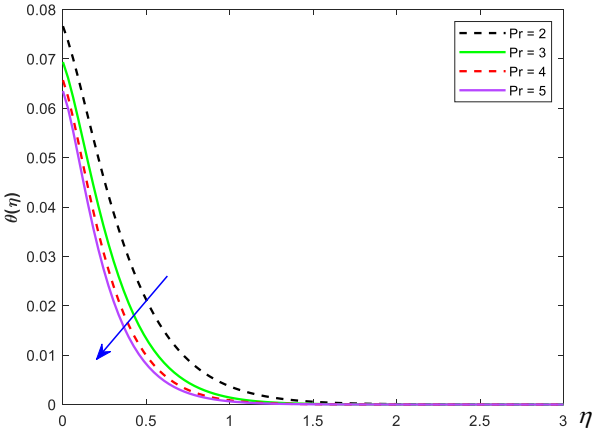

Figure 15. Temperature profiles $\theta(\eta)$ for various Prandtl number Pr when: $\omega = 0.5$; $Ec = 0.1$; $Q = 0.1$; $M = 0.5$; $K = 0.5$; $S = 2.2$; $B = 0.1$; $\lambda = -1$; $\phi_{s1} = 0.01$; $\phi_{s2} = 0.01$.

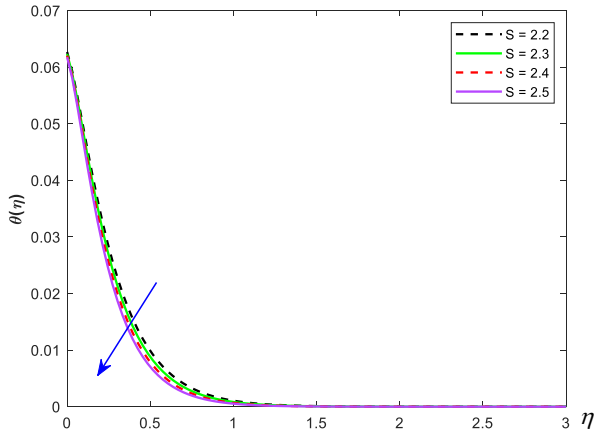

Figure 13. Temperature profiles $\theta(\eta)$ for various suction parameter S when: $\omega = 0.5$; $Ec = 0.1$; $Q = 0.1$; $K = 0.5$; $Pr = 6.2$; $B = 0.1$; $M = 0.5$; $\lambda = -1$; $\phi_{s1} = 0.01$; $\phi_{s2} = 0.01$.

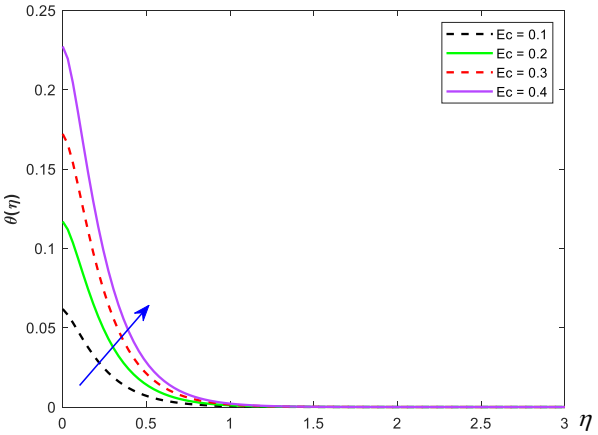

Figure 16. Temperature profiles $\theta(\eta)$ for various Eckert number Ec when: $\omega = 0.5$; $M = 0.5$; $Q = 0.1$; $K = 0.5$; $S = 2.2$; $Pr = 6.2$; $B = 0.1$; $\lambda = -1$; $\phi_{s1} = 0.01$; $\phi_{s2} = 0.01$.

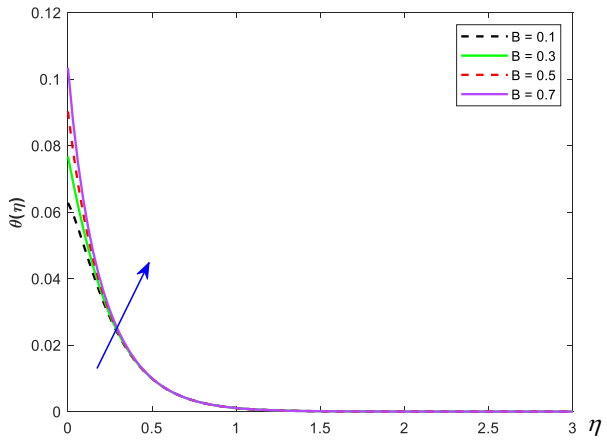

Figure 17. Temperature profiles $\theta(\eta)$ for various Biot number B when: $\omega = 0.5$; $Ec = 0.1$; $Q = 0.1$; $M = 0.5$; $K = 0.5$; $S = 2.2$; $Pr = 6.2$; $\lambda = -1$; $\phi_{s1} = 0.01$; $\phi_{s2} = 0.01$.

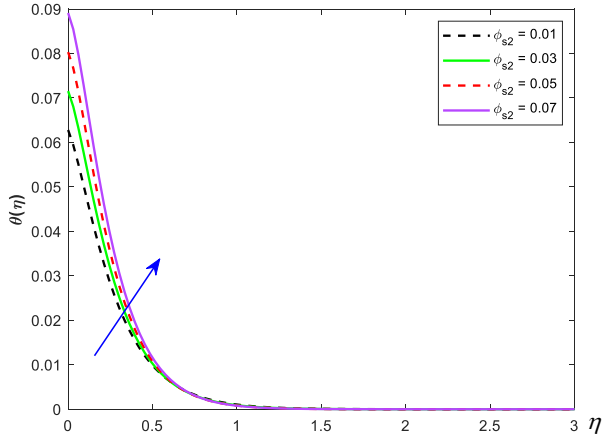

Figure 18. Temperature profiles $\theta(\eta)$ for various volume fraction parameter ϕ_{s2} when: $\omega = 0.5$; $Ec = 0.1$; $Q = 0.1$; $K = 0.5$; $Pr = 6.2$; $B = 0.1$; $M = 0.5$; $\lambda = -1$; $S = 2.2$; $\phi_{s1} = 0.01$.

Impact on local skin friction C_{fx} and C_{fy} and local Nusselt number Nu_x

The suction S effect on the reduced skin friction coefficient $f''(0)$ and $g'(0)$ for various values of copper volume fraction parameter ϕ_{s2} is shown in Figs. 19 and 20. From the figures, it is clear that with increasing values of the copper volume fraction parameter ϕ_{s2} along with the suction param

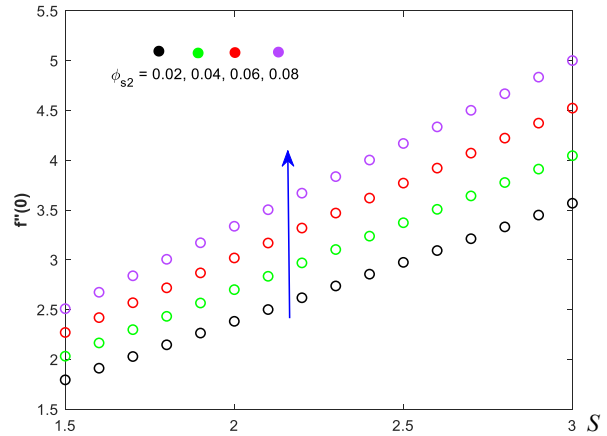

Figure 19. Effect of copper volume fraction ϕ_{s2} with S on $f''(0)$ when: $\omega = 0.5$; $Ec = 0.1$; $Q = 0.1$; $K = 0.5$; $Pr = 6.2$; $B = 0.1$; $M = 0.5$; $\lambda = -1$; $\phi_{s1} = 0.01$.

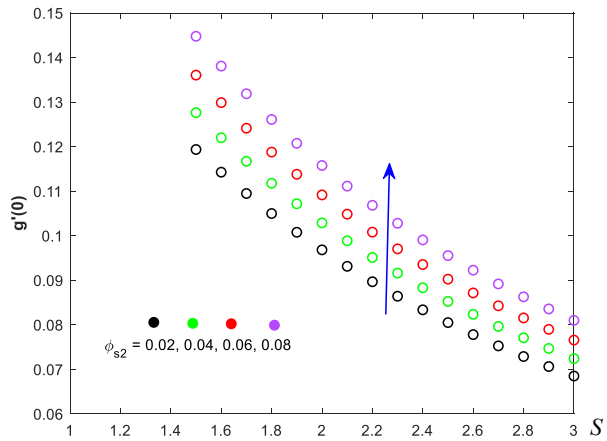

Figure 20. Effect of copper volume fraction ϕ_{s2} with S on $g'(0)$ when: $\omega = 0.5$; $Ec = 0.1$; $Q = 0.1$; $K = 0.5$; $Pr = 6.2$; $B = 0.1$; $M = 0.5$; $\lambda = -1$; $\phi_{s1} = 0.01$.

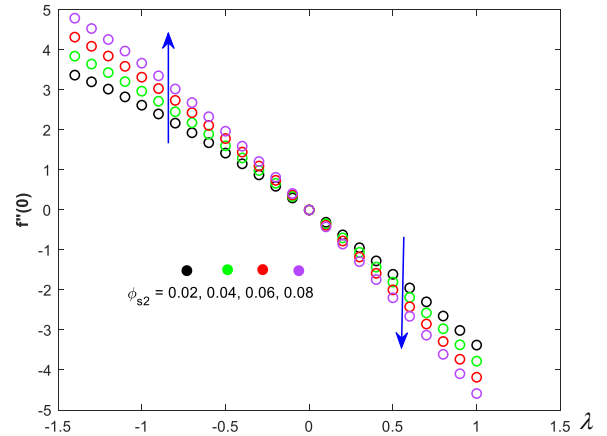

Figure 21. Effect of copper volume fraction ϕ_{s2} with λ on $f''(0)$ when: $\omega = 0.5$; $Ec = 0.1$; $Q = 0.1$; $K = 0.5$; $Pr = 6.2$; $B = 0.1$; $M = 0.5$; $S = 2.2$; $\phi_{s1} = 0.01$.

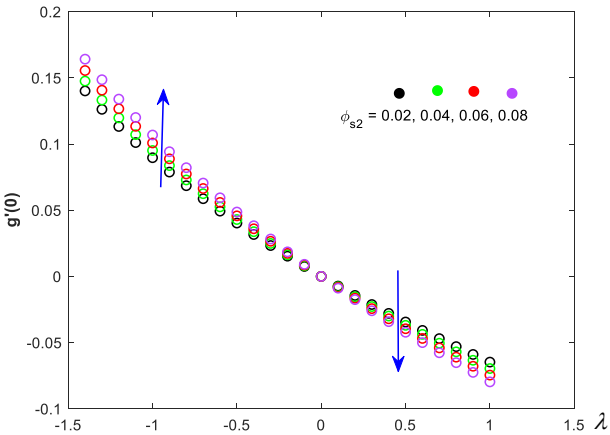

Figure 22. Effect of copper volume fraction ϕ_{s2} with λ on $g'(0)$ when: $\omega = 0.5$; $Ec = 0.1$; $Q = 0.1$; $K = 0.5$; $Pr = 6.2$; $B = 0.1$; $M = 0.5$; $S = 2.2$; $\phi_{s1} = 0.01$.

eter S, the reduced skin friction coefficients $f''(0)$ and $g'(0)$ also increase. A higher quantity of ϕ_{s2} enhances the fluid velocity, resulting in more friction which leads to faster movement and interaction of the solid nanoparticles. In Fig. 21, it is observed that the reduced skin friction coefficient $f''(0)$ increases with increasing value of the copper volume fraction ϕ_{s2} within a certain range ($-1.5 \leq \lambda < 0$) in the

shrinking surface ($\lambda < 0$) region, while the opposite trend occurs in the stretching surface ($\lambda > 0$) region. A similar trend is observed for the skin friction coefficient $g'(0)$ as illustrated in Fig. 22. It is noticed from Fig. 23 that the enhancement of the copper volume fraction ϕ_{s2} along with the suction parameter S reduces the reduced local Nusselt number $-\theta'(0)$. However, the rate of heat transfer reduces in both the stretching and shrinking sheets as the copper volume fraction ϕ_{s2} increases, as illustrated in Fig. 24.

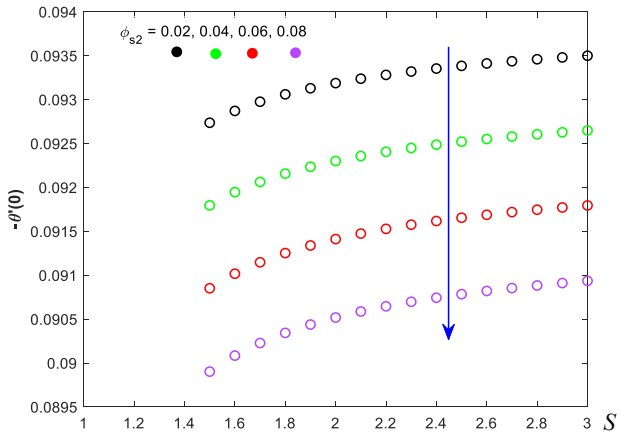

Figure 23. Effect of copper volume fraction ϕ_{s2} with S on $-\theta'(0)$ when: $\omega = 0.5$; $Ec = 0.1$; $Q = 0.1$; $K = 0.5$; $Pr = 6.2$; $B = 0.1$; $M = 0.5$; $\lambda = -1$; $\phi_{s1} = 0.01$.

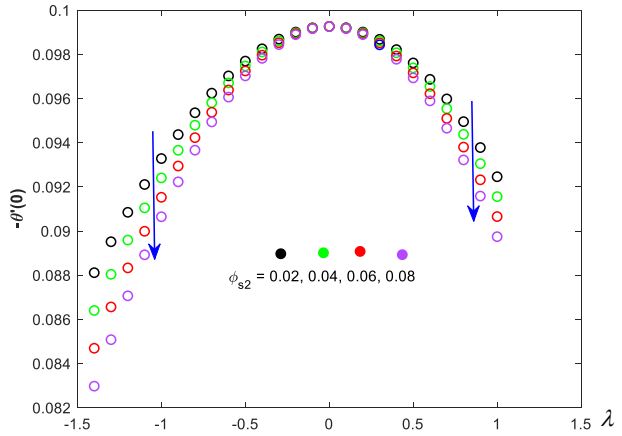

Figure 24. Effect of copper volume fraction ϕ_{s2} with λ on $-\theta'(0)$ when: $\omega = 0.5$; $Ec = 0.1$; $Q = 0.1$; $K = 0.5$; $Pr = 6.2$; $B = 0.1$; $M = 0.5$; $S = 2.2$; $\phi_{s1} = 0.01$.

CONCLUSIONS

The present research focuses on the analysis of three-dimensional rotating flow of convective hybrid nanofluid under the influence of viscous dissipation and heat source effects over a stretching/shrinking permeable sheet in the presence of a magnetic field and heat source. The nanofluid used in the study combines hybrid nanoparticles (Cu-Al_2O_3/water) with a base fluid (H_2O). Numerical solutions are obtained using the bvp4c solver in MATLAB. Key parameters such as velocity profiles $f'(\eta)$ and $g(\eta)$, and temperature profile $\theta(\eta)$ are investigated, and their variations due to governing parameters are depicted through graphical representations. The study also examines the local skin friction coefficient $f''(0)$, $g'(0)$, and reduced Nusselt number $-\theta'(0)$ about the solid copper volume fraction ϕ_{s2}. The main findings of this research include insights as follows.

The study reveals that the magnetic field parameter M has an inverse effect on velocities along x-direction ($f'(\eta)$) and y-direction ($g(\eta)$) and temperature $\theta(\eta)$ profile.

The increasing value of the embedded permeability parameter K enhances both the velocity distribution in x and y-direction.

Thermal boundary layer thickness is uplifted as the quantity of solid copper volume fraction ϕ_{s2}, heat source parameter Q, Eckert number Ec, and Biot number B are increased as a result of the increasing temperature profile.

Enhancement of the solid copper volume fraction ϕ_{s2} enhances the reduced skin friction $f''(0)$ and $g'(0)$ for the suction effect.

Reduced skin friction coefficient $f''(0)$ and $g'(0)$ both increase with solid copper volume fraction ϕ_{s2} with a shrinking sheet, and both decrease with a stretching sheet.

REFERENCES

1. Wang, C.Y. (1988), *Stretching a surface in a rotating fluid.* Z. angew. Math. Phys. 39: 177-185. doi: 10.1007/BF00945764
2. Devi, S.P.A., Devi, S.S.U. (2016), *Numerical investigation of hydromagnetic hybrid Cu-Al2O3/water nanofluid flow over a permeable stretching sheet with suction,* Int. J Nonlin. Sci. Num. Simul. 17(5): 249-257. doi: 10.1515/ijnsns-2016-0037
3. Ramzan, M., Bilal, M., Farooq, U., Chung, J.D. (2016), *Mixed convective radiative flow of second grade nanofluid with convective boundary conditions: An optimal solution*, Results Phys. 6: 796-804. doi: 10.1016/j.rinp.2016.10.011
4. Mustafa, M., Mushtaq, A., Hayat, T., Alsaedi, A. (2016), *Rotating flow of magnetite-water nanofluid over a stretching surface inspired by non-linear thermal radiation*, PLOS One 11(2): e0149304. doi: 10.1371/journal.pone.0149304
5. Hayat, T., Nadeem, S. (2017), *Heat transfer enhancement with Ag-CuO/water hybrid nanofluid*, Results Phys. 7: 2317-2324. doi: 10.1016/j.rinp.2017.06.034
6. Waini, I., Ishak, A., Pop, I. (2019), *Hybrid nanofluid flow and heat transfer over a nonlinear permeable stretching/shrinking surface*, Int. J Numer. Meth. Heat Fluid Flow, 29(9): 3110-3127. doi: 10.1108/HFF-01-2019-0057
7. Wang, F., Tarakaramu, N., Sivakumar, N., et al. (2023), *Three-dimensional nanofluid motion with convective boundary condition in presents of nonlinear thermal radiation via stretching sheet*, J Ind. Chem. Soc. 100(2): 100887. doi: 10.1016/j.jics.2023.100887
8. Hayat, T., Nadeem, S., Khan, A.U. (2018), *Rotating flow of Ag-CuO/water hybrid nanofluid with radiation and partial slip boundary effects*, Eur. Phys. J E, 41(6): 75. doi: 10.1140/epje/i2018-11682-y
9. Aly, E.H., Pop, I. (2019), *MHD flow and heat transfer over a permeable stretching/shrinking sheet in a hybrid nanofluid with a convective boundary condition*, Int. J Num. Methods Heat Fluid Flow, 29(9): 3012-3038. doi: 10.1108/HFF-12-2018-0794
10. Anuar, N.S., Bachok, N., Pop, I. (2021), *Radiative hybrid nanofluid flow past a rotating permeable stretching/shrinking sheet.* Int. J. Num. Methods Heat Fluid Flow, 31(3): 914-932. doi: 10.1108/HFF-03-2020-0149
11. Khashi'ie, N.S., Arifin, N.M., Pop, I., et al. (2020), *Three-dimensional hybrid nanofluid flow and heat transfer past a permeable stretching/shrinking sheet with velocity slip and convective condition*, Chin. J Phys. 66: 157-171. doi: 10.1016/j.cjph.2020.03.032

12. Teh, Y.Y., Asghar, A. (2021), *Three-dimensional MHD hybrid nanofluid flow with rotating stretching/shrinking sheet and Joule heating*, CFD Lett. 13(8): 1-19. doi: 10.37934/cfdl.13.8.119
13. Alias, N.S., Hafidzuddin, M.E.H. (2022), *Effect of suction and MHD induced Navier slip flow due to a non-linear stretching/ shrinking sheet*, Math. Model. Comput. 9(1): 83-91. doi: 10.23 939/mmc2022.01.083
14. Asghar, A., Lund, L.A., Shah, Z., et al. (2022), *Effect of thermal radiation on three-dimensional magnetized rotating flow of a hybrid nanofluid*, Nanomater. 12(9): 1566. doi: 10.3390/nano1 2091566
15. Wahid, N.S., Arifin, N.M., Khashi'ie, N.S., et al. (2022), *Radiative flow of magnetic nanofluid over a moving surface with convective boundary condition.* Math. Model. Comput. 9(4): 791-804. doi: 10.23939/mmc2022.04.791
16. Raju, G., Hari Babu, B., Rama, M.R.L., Varma, S.V.K. (2023), *MHD convective rotating flow of viscoelastic fluid past an infinite vertical oscillating porous plate with Hall effects*, Heat Transf. 52(3): 2277-2294. doi: 10.1002/htj.22784
17. Asghar, A., Vrinceanu, N., Ying, T.Y., et al. (2023), *Dual solutions of convective rotating flow of three-dimensional hybrid nanofluid across the linear stretching/shrinking sheet*, Alex. Eng. J, 75: 297-312. doi: 10.1016/j.aej.2023.05.089